A MODULAR MICROSCOPIC SMARTPHONE ATTACHMENT FOR IMAGING AND QUANTIFICATION OF MULTIPLE FLUORESCENT MICROPARTICLES

By

MUHAMMAD AHSAN SAMI

A thesis submitted to the School of Graduate Studies

Rutgers, The State University of New Jersey In partial fulfillment of the requirements

For the degree of

Master of Science

Graduate Program in Electrical and Computer Engineering

Written under the direction of

Umer Hassan

And approved by

_____

_____

_____

New Brunswick, New Jersey

May 2021

ABSTRACT OF THE THESIS

A Modular Microscopic Smartphone Attachment For Imaging And Quantification Of Multiple Fluorescent Microparticles

by MUHAMMAD AHSAN SAMI

Thesis Director:

Umer Hassan

Portable smartphone-based fluorescent microscopes are becoming popular because of their capability to carry out some of the major functionalities offered by regular benchtop microscopes at a fraction of the cost. However, these smartphone-based microscopes still have a lot of limitations, such as being limited to only one fluorophore, unavailability of multiple magnifications to name a few. To overcome these challenges, we present the design of a modular smartphone-based microscopic attachment. Its modular design allows the user to easily swap between different sets of filters and lenses, thereby providing the choice between multiple fluorophores and magnification levels. Furthermore, our proposed attachment can image specimens on glass slides, cover slips, and microfluidic devices. A 1951 USAF resolution test target was used to quantify the maximum resolution of the microscope which was found to be 3.9 μm.

The performance of the designed smartphone-based fluorescent microscope was then compared with regular benchtop microscope by counting fluorescent microparticles imaged. We found the performance of our design to be satisfactory with an R^2 value of 0.99. Additionally, to automate the quantification of fluorescent microparticles, we developed and trained multiple artificial neural networks (ANNs) using various training

algorithms, and evaluated their performances compared to the control (ImageJ) and found an R^2 value of 0.99. We also performed ANOVA and Tukey's post-hoc analysis and found a p-value=0.97 indicating no significant difference.

As a potential application of the designed smartphone-based microscope, we also developed a PDMS based microfluidic chip to capture and quantify leukocytes from human blood. Anti-human CD45 antibodies were functionalized inside the capture chamber of the microfluidic chip. These antibodies captured cells of interest based on antigen antibody interaction. These captured cells were then made to fluoresce by using a green nuclear stain and the microfluidic chip was imaged under the smartphone based fluorescent microscope.

ACKNOWLEDGEMENTS

I would like to begin by thanking Dr. Umer Hassan for being a great mentor and giving me the opportunity to work under his guidance. His guidance proved invaluable through the course of my thesis project and my Masters' Degree.

I would like to thank the funding support from Department of Electrical and Computer Engineering and Global Health Institute at Rutgers, The State University of New Jersey. I also thank the support from National Science Foundation (Grant Number # 2002511), Office of Naval Research (ONR) (DURIP award # N00014-20-1-2542), Rutgers Vice Chancellor Research Innovation Grant, and Rutgers Global – Collaborative Research Grant

I am thankful to Dr. Chung-Tse Michael Wu and Dr. Mehdi Javanmard for being a part of my Masters' Thesis committee, whose feedback will be immensely helpful. I would like to extend my thanks to John Scafidi, Arletta Hoscilowicz, Pamela Heinold, Christy Lafferty and Kevin Wine.

Special thanks to all the members of my lab: Shreya, Brandon, Kurt, Priya, Hammad, and Pragya for their contributions and timely help. I would also like to thank all my friends from Rutgers Makerspace, especially Dan, who helped and taught me a lot about 3D printing and laser cutting techniques.

I would also like to thank all my wonderful friends Ahsan, Aunns, Baber, Tayyab, and Zarak for always being there for me. I am only writing it here because I know that none of you will ever bother to go through my thesis.

I would like to mention my family, Mohsin, Hassan, Lala, and my parents, Dr. Sami Ullah and Dr. Saliah Gul. Without you, there is no way that I would have come this far in my life. This is all because of you! I hope I can make you proud someday. I would also like to thank my fiancé, Eman for being a very important part of my life. Finally, I would like to thank my Creator for giving me the knowledge, wisdom and His blessings throughout my life.

TABLE OF CONTENTS

LIST OF FIGURES

1. INTRODUCTION

1.1 Introduction to fluorescent microscopy

Fluorescent microscopy is an advanced type of microscopy that finds particular importance in the fields of biology and material science [1][2]. It enables the identification of cells and cellular components with a great deal of precision. By tagging the specimen with multiple different probes, fluorescent microscopy can simultaneously identify several target molecules [3][4]. Though modern microscopes are equipped with a lot of functional modalities, they can cost the user thousands of dollars and are heavy as well. Recently, researchers have been working a lot on developing smartphone-based microscopes to provide a low cost, portable, and efficient alternative to the traditional bulky benchtop microscopes [5].

1.2 Smartphone based fluorescent microscopes

Smartphone-based fluorescent microscopes (SBFMs) have a great potential for being used as point of care platforms for diagnostics, healthcare, and environmental monitoring [6]. Modern smartphones are equipped with cutting edge camera units which allow for the capture of high quality and detailed images. SBFMs have been employed in a wide range of settings that include the detection of different biomarkers including proteins and nucleic acids [7][8][9][10]11]. Ozcan et.al reported the quantification of red and white blood cells as well as hemoglobulin from whole blood using a smartphone-based

microscope [12]. Moreover, SBFMs have also been employed for the detection of parasites as well as for the imaging single nanoparticles and viruses [13][14]. Researchers discussed the design and working of a multi-color smartphone-based fluorescence microscope capable of imaging two fluorophores at two magnification levels [15]. Researchers reported the use of colored lenses along with smartphones to image multiple fluorophores [16]. SBFMs have also been used for monitoring drug-induced nephrotoxicity on an organ on chip (OOC) [17]. Lee et al. demonstrated the adaptation of a smartphone's camera to function as a compact lens less microscope using ambient light [18]. The method is based on the shadow imaging technique where the sample is placed on the surface of the image sensor, which captures direct shadow images under illumination. A hand-held smartphone based quantitative phase microscope using the transport of intensity equation method has also been demonstrated [19]. Jung et al. presented a portable multi-contrast microscope operating on a smartphone platform [20]. Based on color-multiplexing of illumination angles, the microscope enabled acquisition of Bright Field, Dark Field, and Differential Phase Contrast images in a single shot. Identification of fluorescently labelled pathogenic bacteria has been recently demonstrated using a SBFM [21]. Knowlton et al. developed a SBFM incorporating magnetic focusing technology to increase the application of the platform to a broad range of biomedical assays [22]. Moreover, they have also been employed in multiple global health ventures for the diagnosis of diseases in the developing world. In our past studies, we have also used a biochip in conjunction with SBFMs for quantification of nCD64 and

leukocytes at POC [23][24].

1.3 Statement of problem

Although a lot of work has been done in the development of SBFMs, a lot more still needs to be done. An ideal SBFM should be able to mimic the basic functionality of a benchtop microscope by being able to image multiple fluorophores and offer the user different levels of magnifications. There is however more to this story. With more than 1.5 billion new smartphones getting sold every year [25], SBFMs have got to be generic in nature and not limited to usage with just one device. Furthermore, they should offer at least some level of compatibility with microfluidic devices and not just be limited to imaging specimens on a glass slide. To the best of our knowledge, no such SBFM has yet been reported which satisfies all the above-mentioned criteria.

1.4 Research goals

In this work, we present the design and working of a modular SBFM that satisfies the criteria mentioned above. The said SBFM is capable of working with a multitude of smartphones and is not limited to only one for usage [26]. The lens used for creating the necessary magnification and the filters employed for creating the necessary darkfield image are all easily replaceable. This allows our SBFM to work with multiple fluorophores and capture images at multiple magnification levels as desired by the user. We have imaged human peripheral blood leukocytes and polystyrene beads tagged with green and red fluorophores using the said setup at two different magnification levels. Furthermore, to

automate the quantification process of the imaged beads and leukocytes, we developed an artificial neural network (ANN) based algorithm. The ANN was trained through multiple training algorithms and its performance was compared to the particle counts obtained from the control (ImageJ). We also performed statistical analysis to determine if there was a statistically significant difference between the counts predicted from the ANN based algorithm and the control [26]. Lastly, as a potential application, we conducted some preliminary experiments to quantify leukocytes using a PDMS based microfluidic chip in conjunction with the SBFM.

1.5 Thesis organization

In chapter 2 we have highlighted the different materials, reagents, and the experimental setups that were used in this study during the design and evaluation of the presented SBFM. In chapter 3, we have presented the results of the SBFMs performance and how it compares to the existing benchtop fluorescent microscopes. In chapter 4, we shown the results obtained for the quantification of peripheral blood leukocytes. In chapter 5, we have summarized our findings and have drawn conclusions and outlined the future scope of the project.

2. DESIGN AND EVALUATION OF THE PRPOSED MICROSCOPE

2.1 Design of smartphone-based fluorescent microscope

Since the microparticles were going to be imaged using fluorescence microscopy, we designed our attachment in such a way so as ensure that no external photons reach the imaging cavity. To do so, we divided the attachment into two portions, a top portion and a bottom portion. The glass slide or the microfluidic chip with the captured leukocytes is placed inside the attachment and therefore, no external pump photons can enter the imaging portion. A cover shield is placed on top of the microfluidic chip placed in the bottom chamber to minimize the leakage of light reflecting from the walls of the attachment present around the chip. For green fluorophores, a set of three blue LED's (Product no: 516-2800-1-ND) from Digi Key corporation are used while for the red fluorophores, green LED's were procured from Adafruit (Product ID: 300) are used.

A bandpass fitter for the excitation LED's is placed in the bottom portion and the high pass filter is placed on the top portion along with the lens. A bandpass filter with a center wavelength of 470 nm and bandwidth of ~40 nm (Chroma Inc. ,Product no. ET470/40x) is used as an excitation filter for blue LED's and for green LED's, a bandpass filter with 535 nm centre wavelength and bandwidth of 50 nm (Chroma Inc. ,Product no. ET535/50m) is used. When working with green fluorophores, a long pass filter with a cut-off value of 500 nm (Semrock, Product no: FF01-500/LP-23.3-D) is used, whereas, in case of red fluorophores, a long pass filter with a cut-off value of 593 nm (Semrock, Product no: FF01-593/LP-25) is used.

The magnification lens, along with both the filters can be swapped with different ones depending on the requirements. We procured two lenses with different focal

length from Edmund optics to offer multiple magnification levels to the user. One lens had a focal length of 10 mm while the other had a focal length of 15 mm. To help focusing on the imaging plane, four screws have been placed on the corners of the smartphone attachment which, when rotated can manipulate the distance between the top and bottom portion of the attachment and help in focusing on the right imaging plane. The computer aided design (CAD) of the smartphone based fluorescent microscope is shown in Figure 2.1 below.

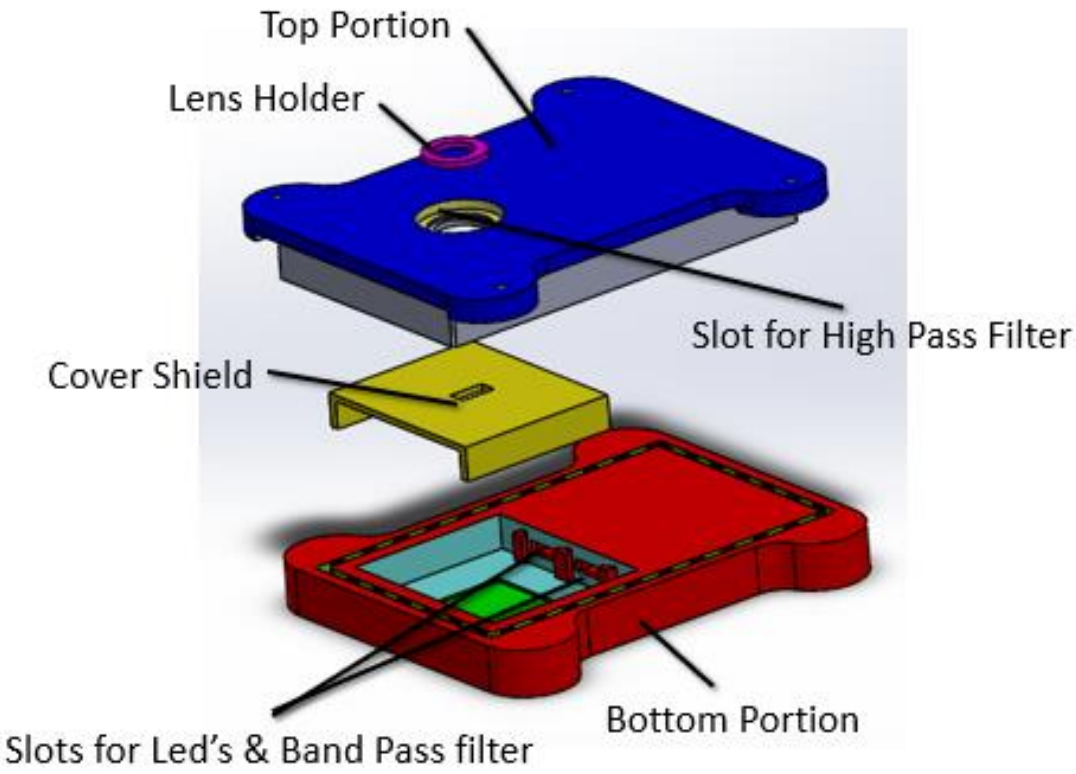

Figure 2-1 Disbanded 3D CAD Model of the designed microscopic smartphone based fluorescent microscope.

We then 3D printed the designed smartphone based fluorescent microscope. For the said purpose, Markforged printer was used and onyx was used as the printing material. Figure 2.2 below show the 3D printed SBFM working along with

Samsung Galaxy S9+.

Figure 2-2 3D printed smartphone based fluorescent microscope working in conjunctions with a Samsung Galaxy S9+. Reproduced from Ref. [26] with permission from the Royal Society of Chemistry.

2.2 Optical resolution offered by SBFM:

The optical resolution of the SBFM was evaluated using both Galaxy S9+ and Lumia 1020. With both smartphones, the 10 mm focal length lens was used, and the 1951 USAF resolution test chart was imaged. With Lumia 1020, we were able to resolve the lines of Group 7 element 1 which pointed to a resolution of 3.9 µm. Figure 2.3 below showcases the 1951 USAF resolution test chart when imaged using Lumia 1020.

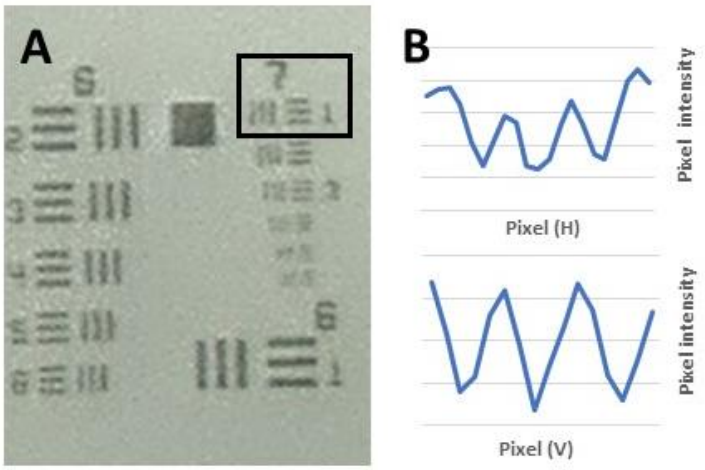

Figure 2-3 1951 USAF resolution test chart imaged using Lumia 1020 and 10 mm focal length lens. (b) Image pixel intensity. Reproduced from Ref. [26] with permission from the Royal Society of Chemistry.

We also imaged the 1951 USAF resolution test chart using the Samsung galaxy S9+ using the 10 mm focal length external lens and were able to resolve the lines of Group 6 element 3. This corresponds to an optical resolution of 6.2 µm. Figure 2.4 below showcases the 1951 USAF resolution test chart when imaged using Samsung Galaxy S9+.

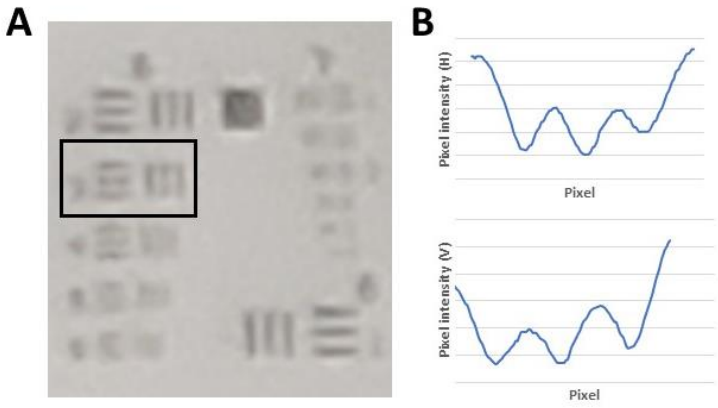

Figure 2-4 1951 USAF resolution test chart imaged using Galaxy S9+ and 10 mm focal length lens. (b) Image pixel intensity. Reproduced from Ref. [26] with permission from the Royal Society of Chemistry.

2.3 Green fluorescent microbead imaging on SBFM

Green fluorescent microbeads with a mean diameter of 8.3 µm were acquired from Banglabs. These specific beads were chosen because they are somewhat similar in size when compared to human leukocytes. For the green beads, a long pass filter with a cut-off value of 500 nm was used along with lens of 15 mm focal length for imaging. 1X PBS buffer was used to create different concentrations of the beads for imaging. 2 µl sample from each concentration was then poured on a glass slide and placed inside the smartphone setup for imaging. The fluorescent beads were excited using the light emitted by the smartphone setup's blue LED's and Imaged by a Samsung Galaxy S9+.

2.4 Red fluorescent microbead imaging on SBFM

Red fluorescent microbeads with a mean diameter of 10 µm were acquired from Thermofisher scientific. For the red beads, long pass filter with a cut-off value of 593 nm was used along with lens of 15 mm focal length for imaging. 1X PBS buffer was used to create different concentrations of the beads for imaging. 2 µl sample from each concentration was then poured on a glass slide and placed inside the smartphone setup for imaging. The red beads were excited using the green LED's of the SBFM and Imaged by a Samsung Galaxy S9+.

2.5 Leukocyte imaging using the SBFM

RBC lysis buffer media from ThermoFisher was used to lyse the red blood cells in peripheral human blood. The isolated leukocytes need to fluoresce for successful imaging using the SBFM. In order to make them fluoresce, we used a green nuclear stain, which made the isolated leukocytes fluoresce for imaging using the SBFM. Stock solution for the nuclear stain was prepared by adding 3 µl of SYTO 16, (ThermoFisher Scientific, Catalogue Number: S7578), in 1 ml

of 1X PBS. SYTO 16 stock solution and the isolated leukocytes were then added in a 1:1 ratio in a 1.5 ml Eppendorf tube and were incubated in dark for 15 minutes at room temperature. 1X PBS buffer was used to create different concentrations of the fluorescent leukocytes for imaging. 2 µl sample from each concentration was then poured on a glass slide and placed inside the smartphone setup for imaging. Since the fluorescent leukocytes were green in color, they were excited using the light emitted by the smartphone setup's blue LED's and Imaged by a Samsung Galaxy S9+ coupled with a long pass filter with a cut-off value of 500 nm, and a lens of 15 mm focal length

2.6 Fluorescent microparticles imaged by SBFM:

As explained above, both green and red fluorescent particles were imaged using the SBFM. In order to switch between the red ang green fluorophores, the user has to change long pass filter which is placed on the top portion of the SBFM. Because of its modular design, this can be done easily and does not require any trainings. The images of red and green fluorescent microparticles obtained by the SBFM when used in conjunction with galaxy S9+ are shown below in Figure 2.5.

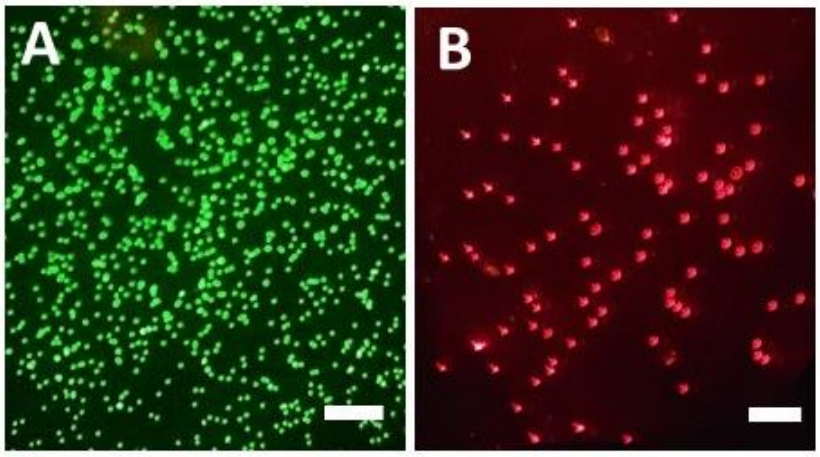

Figure 2-5 Green fluorescent microparticles imaged using the SBFM along with a Galaxy S9+. (b) Red fluorescent microparticles imaged using the SBFM along with a Galaxy S9+. (Scale bar = 100 μm). Reproduced from Ref. [26] with permission from the Royal Society of Chemistry.

2.7 Multiple magnification options offered by SBFM

In microscopy, sometimes a larger magnification is needed whereas in some a larger field of view (FOV) offers more information. The designed SBFM allows the user to choose between multiple magnification settings. To do so, the user simply has to swap between the two lenses. The lens with a focal length of 15 mm offers a larger FOV whereas the one with a focal length of 10 mm offers a higher magnification. The ability to choose between the two is therefore very important. Figure 2.6 shows the maximum magnification offered by SBFM for green microparticles when lens with 15 mm focal length is being used, and the dotted region 1 showcases the maximum available magnification when using lens with 10 mm focal length is used.

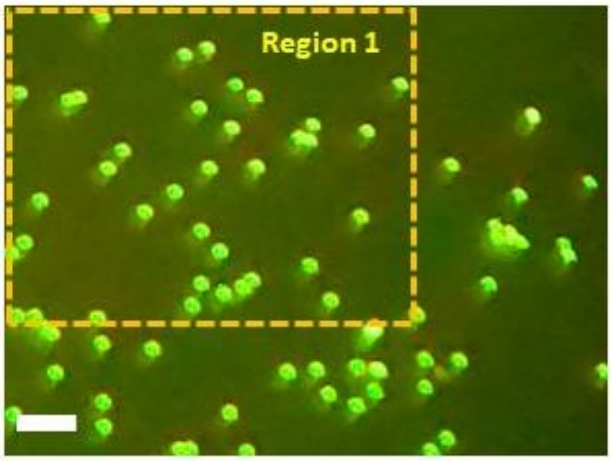

Figure 2-6 Green fluorescent particles imaged using 15 mm focal length lens at maximum zoom offered by smartphone. Region 1 shows the green fluorescent particles imaged using 10 mm focal length lens at maximum zoom offered by smartphone (Scale bar = 50μm). Reproduced from Ref. [26] with permission from the Royal Society of Chemistry.

We also evaluated the multiple zoom feature offered by the SBFM when used in conjunction with red microparticles and the results are shown in Figure 2.7 below.

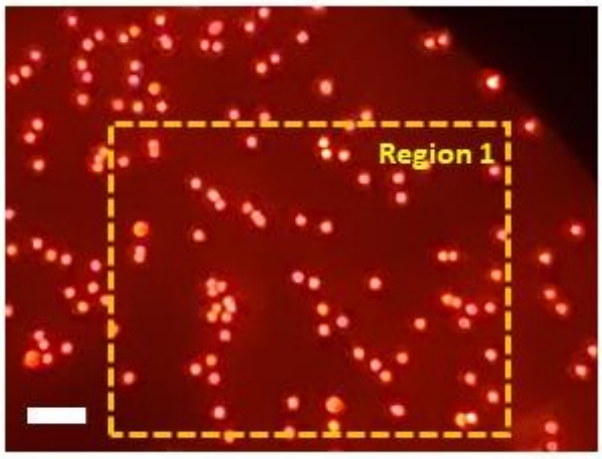

Figure 2-7 Red fluorescent particles imaged using 15 mm focal length lens at maximum zoom offered by smartphone. Region 1 shows the red fluorescent

particles imaged using 10 mm focal length lens at maximum zoom offered by smartphone (Scale bar = 50μm). Reproduced from Ref. [26] with permission from the Royal Society of Chemistry.

2.8 Particle quantification using ImageJ

ImageJ was used a control method for quantifying the beads and leukocytes imaged through the SBFM and the regular benchtop fluorescent microscope. As a first step, the obtained images are first converted into 8-bit format and then the regions of interest are encapsulated using the thresholding function. The pixel size and the circularity range are then provided to get the final particle count. Because the fluorescent microparticles are not completely circular in nature, we kept the circularity in a range of 0.6 to 1, 1 representing a perfect circle. Figure 2.8 showcases a flowchart which represents the different steps involved in getting particle counts using ImageJ from any image.

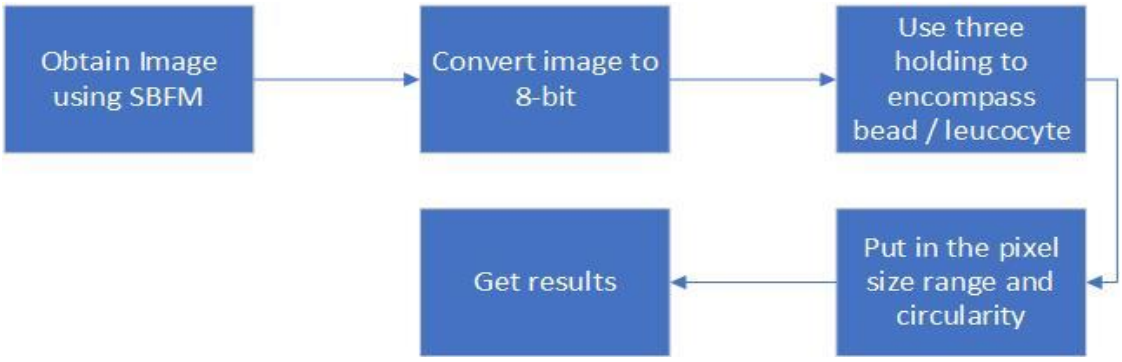

Figure 2-8 Flowchart showcasing the steps involved in obtaining leukocyte/bead count from any image using ImageJ. Reproduced from Ref. [26] with permission from the Royal Society of Chemistry.

2.9 Performance evaluation of SBFM

The fluorescent microparticles imaged using the SBFM were also imaged using the benchtop fluorescent microscope. This was done to draw a comparison between the performance efficiency of the SBFM and the benchtop fluorescent microscope. Images from both the benchtop microscope and the SBFM were then quantified using ImageJ and a correlation plot was drawn. We can see the SBFM works almost just as good as the benchtop microscope based on the plot shown in Figure 2.9. An R^2 value of 0.99 shows a very good correlation. We also did the Bland Altman analysis of this data and the results are shown in Figure 2.10.

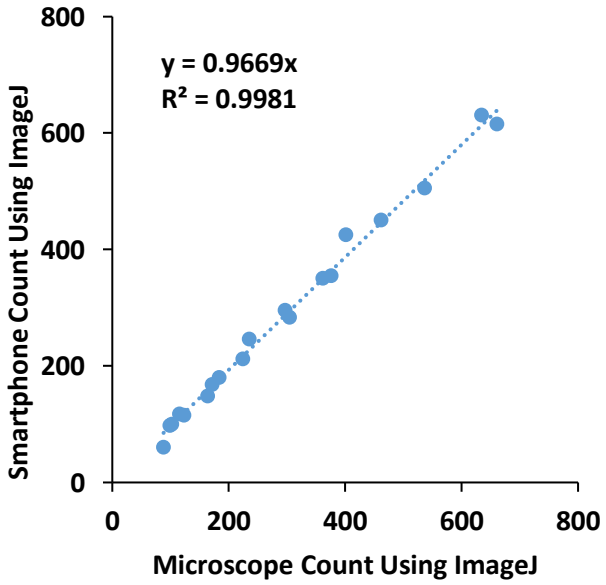

Figure 2-9 Correlation plot between the particle counts obtained using the SBFM and the regular benchtop microscope. Reproduced from Ref. [26] with permission from the Royal Society of Chemistry.

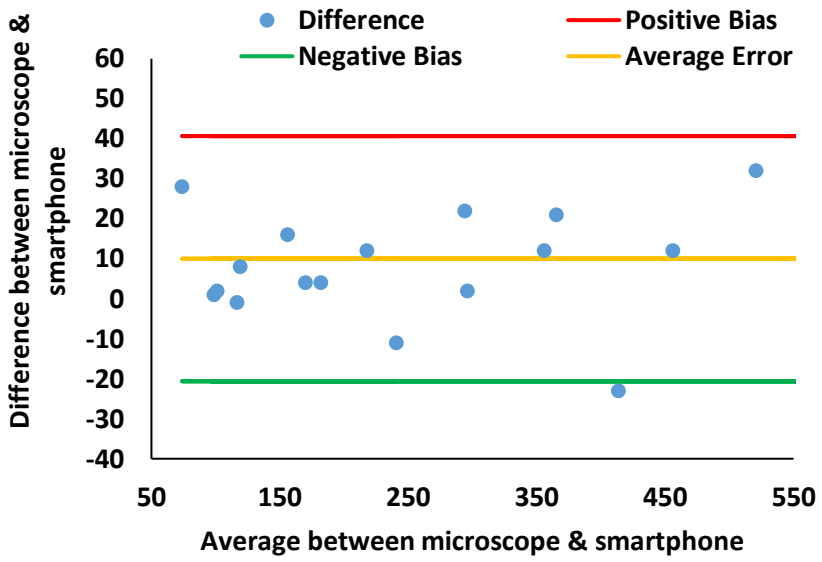

Figure 2-10 Bland Altman analysis of the particle counts obtained using the SBFM and the regular benchtop microscope. Reproduced from Ref. [26] with permission from the Royal Society of Chemistry.

3. ARTIFICAL NEURAL NETWORKS FOR IMAGE PROCESSING

We also analyzed the bead and leukocyte images obtained from the SBFM using the MATLAB based artificial neural networks. A two-layer feed-forward artificial neural network with 10 hidden neurons for hidden layer and 1 neuron for output layer was used for the said purpose. This network was then trained using different methods including Levenberg Marquardt, scaled conjugate gradient, and Bayesian regularization, and for each method, ten different networks were trained.

3.1 Quantification of microparticles using artificial neural networks

The image processing algorithm was developed on MATLAB and is based on

the imfindcircles function. It takes in the size range of the particles to quantified as inputs and generates 10 possible counts for different sensitivity values. Afterwards, multivariate regression was performed on this data obtained through the imfindcircles using artificial neural networks in MATLAB. The network diagram of the double layer feed forward artificial neural network with sigmoid neurons and softmax output is shown in Figure 3.1.

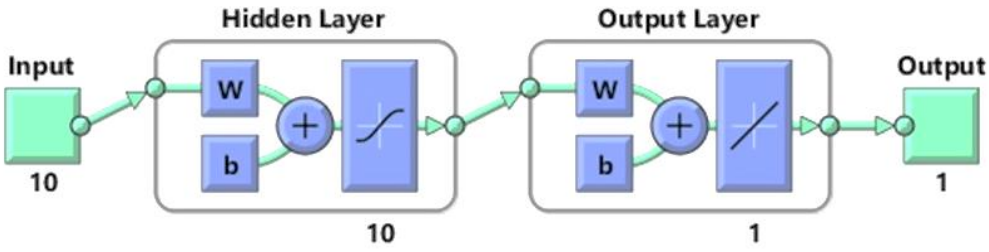

Figure 3-1 The network diagram of the feed forward artificial neural network with sigmoid hidden and softmax output neurons. Reproduced from Ref. [26] with permission from the Royal Society of Chemistry.

The designed neural network consisted of 10 neurons (hidden layer) and 1 neuron (output layer). The input to the neural network contains the 10 counts generated by imfindcircles for different sensitivity values. Using these, the network then predicts the final microparticle count count. For training the neural network, 93 SBFM images were used.

Three different training methods were used to train the artificial neural network. For each of the three training methods, we created ten different networks resulting in a of 30 networks. Levenberg Marquardt method for training the networks first, it takes more memory but less time to train. When Levenberg Marquardt method is used, the training stops when there is no improvement in generalization which is also indicated by an increase in the mean squared error of samples. Afterwards, scaled conjugate gradient method was used for training.

Scaled conjugate gradient method takes the least memory of all the methods we used. In case of scaled conjugate gradient method, the training stops when there is no improvement in generalization, which is also indicated by an increase in the mean squared error of samples. Finally, we used Bayesian regularization method. Bayesian regularization method takes more time to train but offers better prediction accuracy. In Bayesian regularization, training is stopped on the basis of a regularization protocol. The flowchart shown in Figure 3.2 showcases the process of getting counts from SBFM images using the developed ANN.

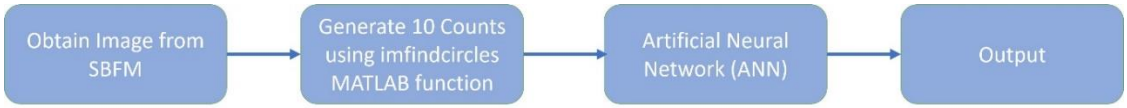

Figure 3-2 Flowchart showcasing the steps involved in obtaining leukocyte/bead count from any image using the developed ANNs. Reproduced from Ref. [26] with permission from the Royal Society of Chemistry.

Performance of these trained networks was then evaluated by exposing them to new images obtained from the SBFM and by comparing their predictions to the control count obtained through ImageJ. Afterwards, we picked the top three performing ANN for a closer evaluation.

3.1.1 ANN 1 trained using scale conjugate gradient method

This ANN was trained using SCG method. The Hinton diagram of the network is shown below in Figure 3.3 while the training parameters of this networks are shown in Figure 3.4 and 3.5.

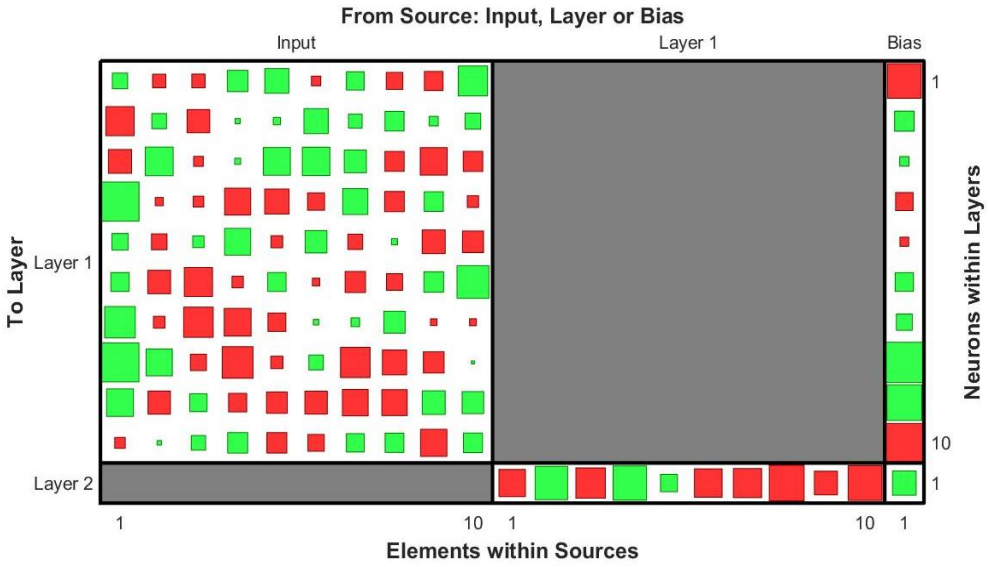

Figure 3-3 Hinton diagram representing the weight and bias values of the input (hidden) layers and output layers of neurons in our neural network that was trained using scaled conjugate gradient method. Reproduced from Ref. [26] with permission from the Royal Society of Chemistry.

Now we looked more closely into the counts that were predicted by this ANN on the ten completely unseen images obtained from the SBFM. We then plotted them against the counts predicted by ImageJ and obtained the R^2 value. The correlation plot is shown in Figure 3.6.

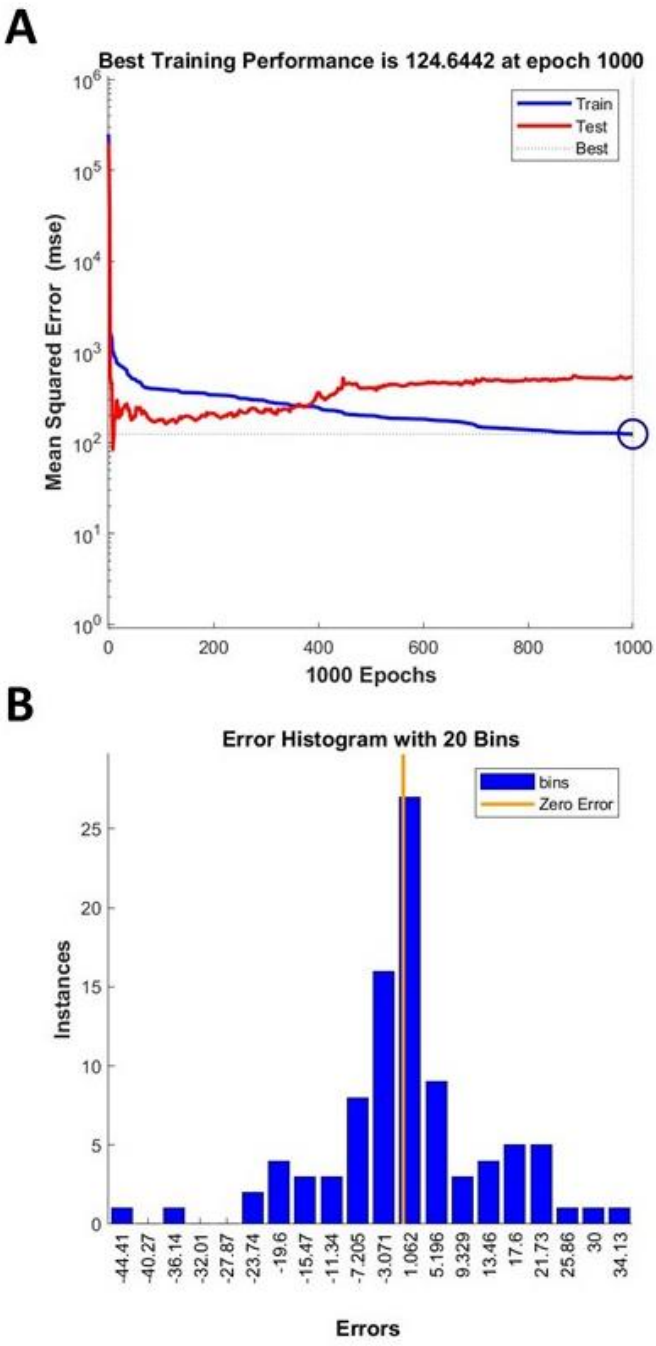

Figure 3-4 First artificial neural network performance using scaled conjugate gradient method for training. (a) mean squared error at different epochs. (b) the error histogram of the model. Reproduced from Ref. [26] with permission from the Royal Society of Chemistry.

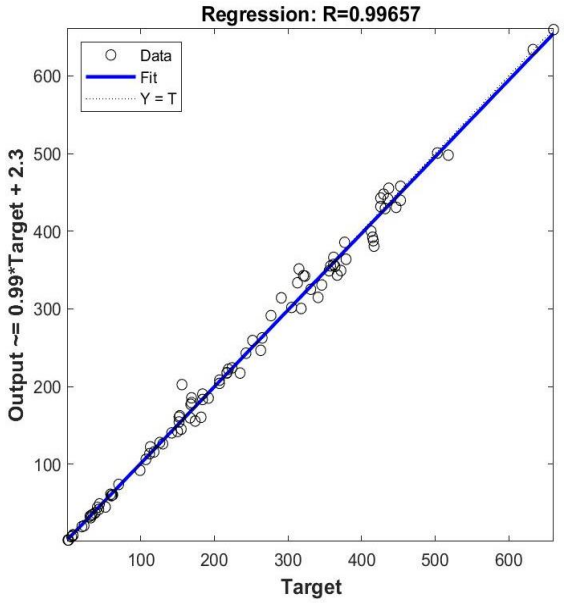

Figure 3-5 The network was trained using scaled conjugate gradient algorithm and the resulting regression plot consisting of training, validation, and testing. Reproduced from Ref. [26] with permission from the Royal Society of Chemistry.

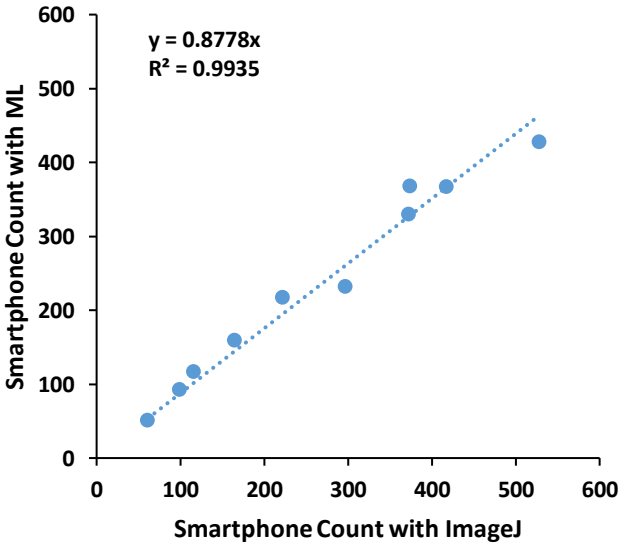

Figure 3-6 Correlation plot between the particle counts obtained using ANN and the control (ImageJ). Reproduced from Ref. [26] with permission from the Royal Society of Chemistry.

3.1.2 ANN 2 trained using scale conjugate gradient method

This ANN was also trained using SCG method. The Hinton diagram of the network is shown below in Figure 3.7 while the training parameters of this networks are shown in Figure 3.8 and 3.9.

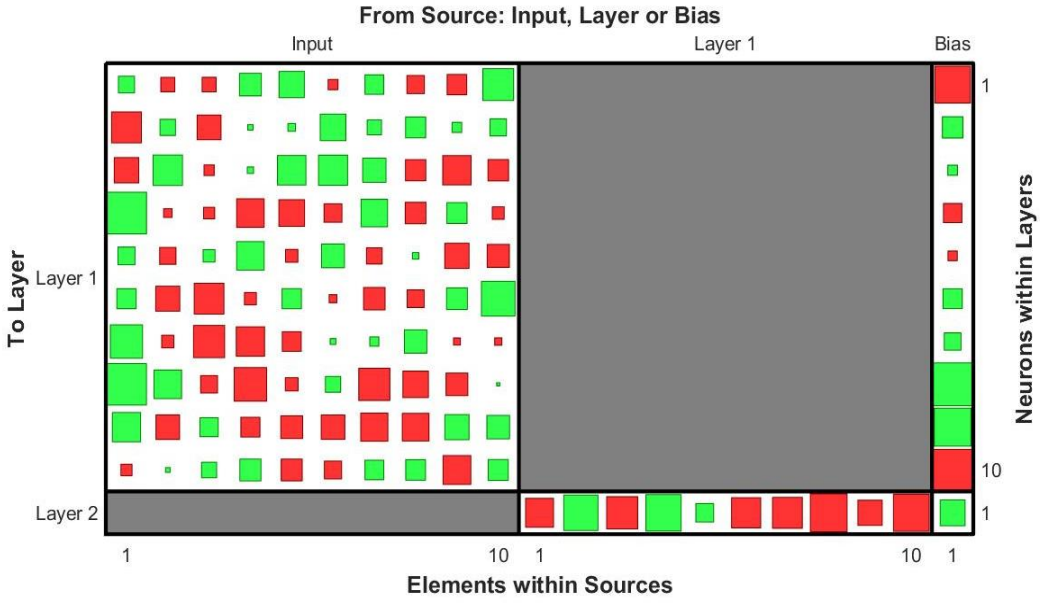

Figure 3-7 Hinton diagram representing the weight and bias values of the input (hidden) layers and output layers of neurons in our neural network that was trained using scaled conjugate gradient method. Reproduced from Ref. [26] with permission from the Royal Society of Chemistry.

Now we looked more closely into the counts that were predicted by this ANN on the ten completely unseen images obtained from the SBFM. We then plotted them against the counts predicted by ImageJ and obtained the R^2 value. The correlation plot is shown in Figure 3.10.

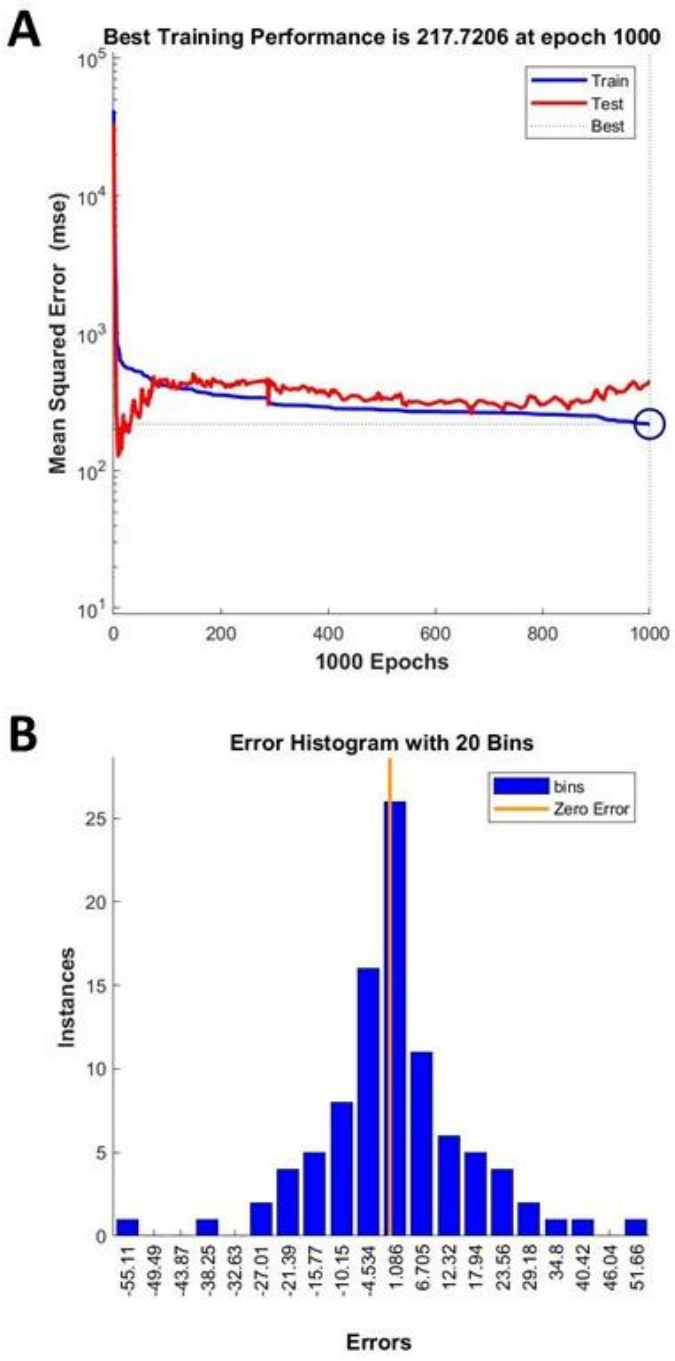

Figure 3-8 Second artificial neural network performance using scaled conjugate gradient method for training. (a) mean squared error at different epochs. (b) the error histogram of the model. Reproduced from Ref. [26] with permission from the Royal Society of Chemistry.

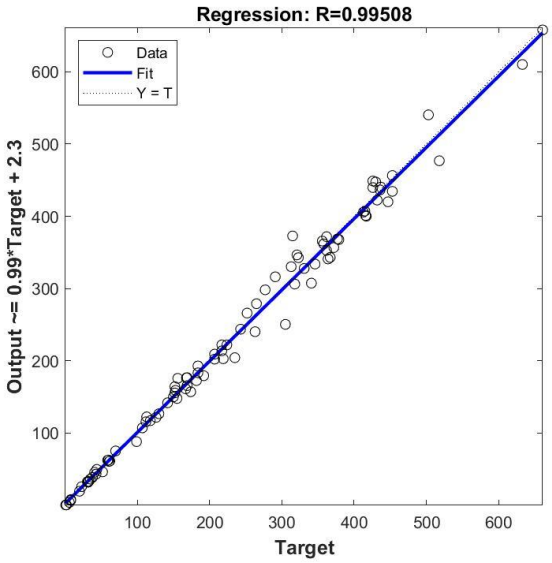

Figure 3-9 The network was trained using scaled conjugate gradient algorithm and the resulting regression plot consisting of training, validation, and testing is shown. Reproduced from Ref. [26] with permission from the Royal Society of Chemistry.

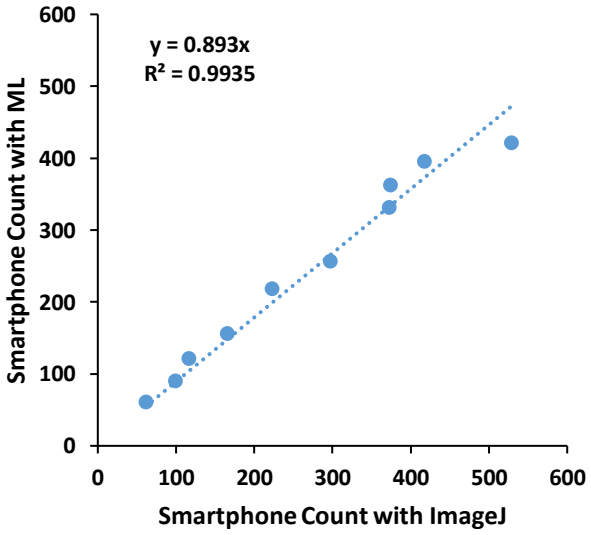

Figure 3-10 Correlation plot between the particle counts obtained using ANN and the control (ImageJ). Reproduced from Ref. [26] with permission from the Royal Society of Chemistry.

3.1.3 ANN 3 trained using Bayesian regularization method

This ANN was also trained using BR method. The Hinton diagram of the network is shown below in Figure 3.11 while the training parameters of this networks are shown in Figure 3.12 and 3.13.

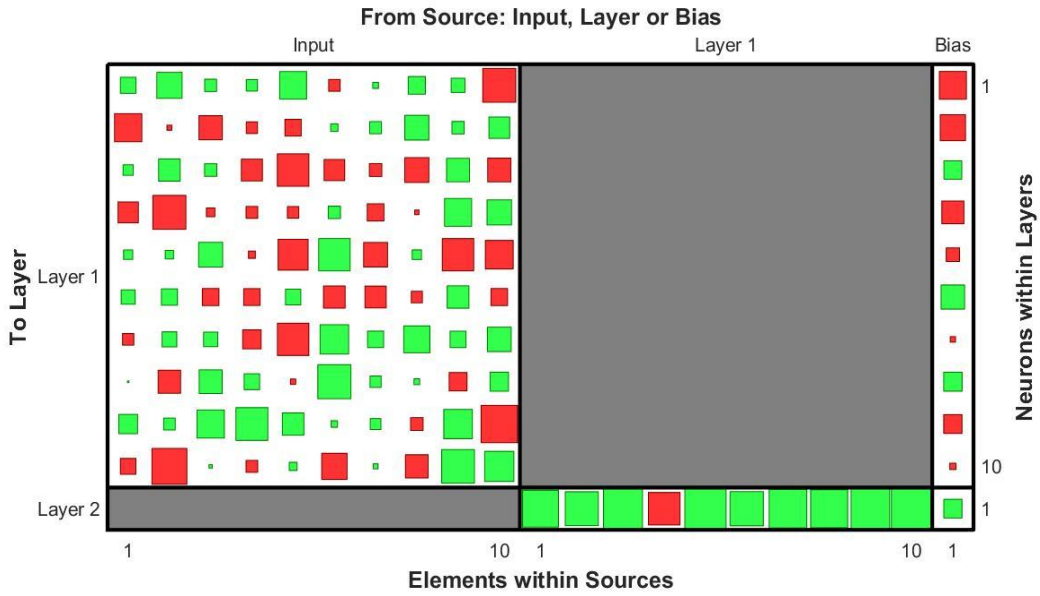

Figure 3-11 Hinton diagram representing the weight and bias values of the input (hidden) layers and output layers of neurons in our neural network that was trained using Bayesian method. Reproduced from Ref. [26] with permission from the Royal Society of Chemistry.

Now we looked more closely into the counts that were predicted by this ANN on the ten completely unseen images obtained from the SBFM. We then plotted them against the counts predicted by ImageJ and obtained the R^2 value. The correlation plot is shown in Figure 3.14.

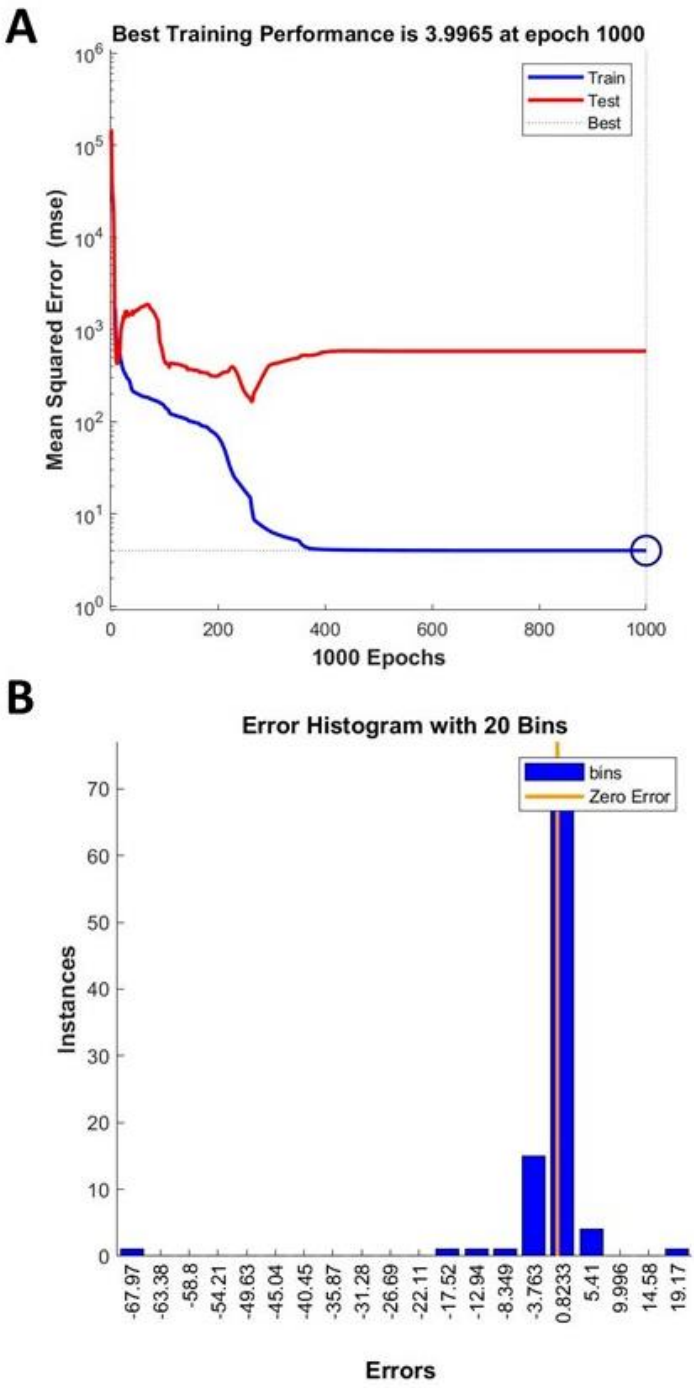

Figure 3-12 Third artificial neural network performance using Bayesian regularization method for training. (a) mean squared error at different epochs. (b) the error histogram of the model. Reproduced from Ref. [26] with permission from the Royal Society of Chemistry.

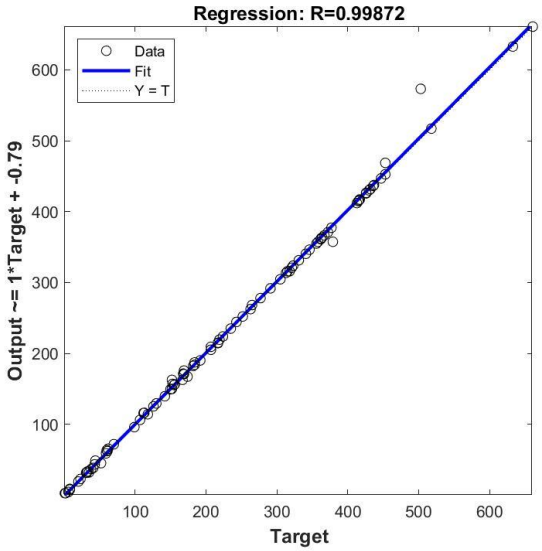

Figure 3-13 The network was trained using scaled Bayesian regularization and the resulting regression plot consisting of training, validation, and testing is shown. Reproduced from Ref. [26] with permission from the Royal Society of Chemistry.

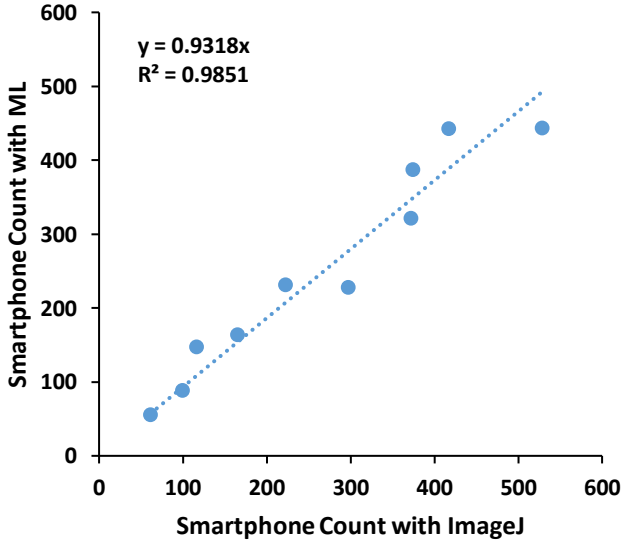

Figure 3-14 Correlation plot between the particle counts obtained using ANN and the control (ImageJ). Reproduced from Ref. [26] with permission from the Royal Society of Chemistry.

3.2 Statistical Analysis

We also did some statistical tests on R to determine if there was a significant difference in the counts predicted by the ANNs and the control. The Shapiro-Wilk tests yielded the values: (W=0.94691, p-value=0.6321) for ImageJ, (W=0.93759, p-value=0.5266) for Scaled Conjugate Gradient 1(SCG1), (W=0.93105, p-value=0.4583) for Scaled Conjugate Gradient 2(SCG2), and (W=0.92748, p-value=0.4236) for Bayesian Regularization(BR) which meant all the data was normal. Bartlett's test gave a p-value of 0.95 showing that nor significant difference existed among the variances of the data sets. We then applied ANOVA which gave a p-value of 0.97 showing no significant difference the data sets. For better visualization and individual comparison, we did Tukey's test which showed no significant difference as well. The Tukey's test result is shown in Figure 3.15. For all the analyses, a significance level of ($\alpha = 0.05$) was used.

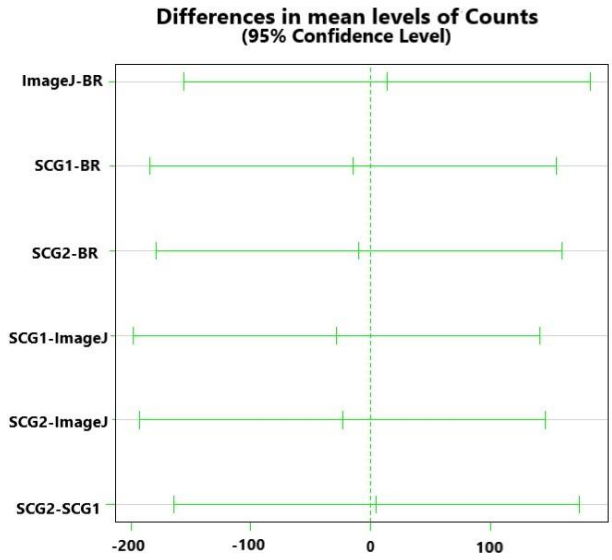

Figure 3-15 Tukey plot of the data shown obtained through the different ANNs and the control method ImageJ Reproduced from Ref. [26] with permission from the Royal Society of Chemistry.

3.3 ANN analysis time

Using MATLAB, we evaluated the time taken for the developed ANN to quantify the number of particles in the image obtained from the SBFM. To do so, we used the tic toc function of MATLAB. Images of fluorescent microparticles were obtained using Samsung Galaxy S9+, iPhone XS, and Nokia Lumia 1020 at the minimum and maximum digital zoom on different aspect ratios. The time taken by the ANN to quantify the microparticles in these images was then calculated and is shown in Figure 3.16.

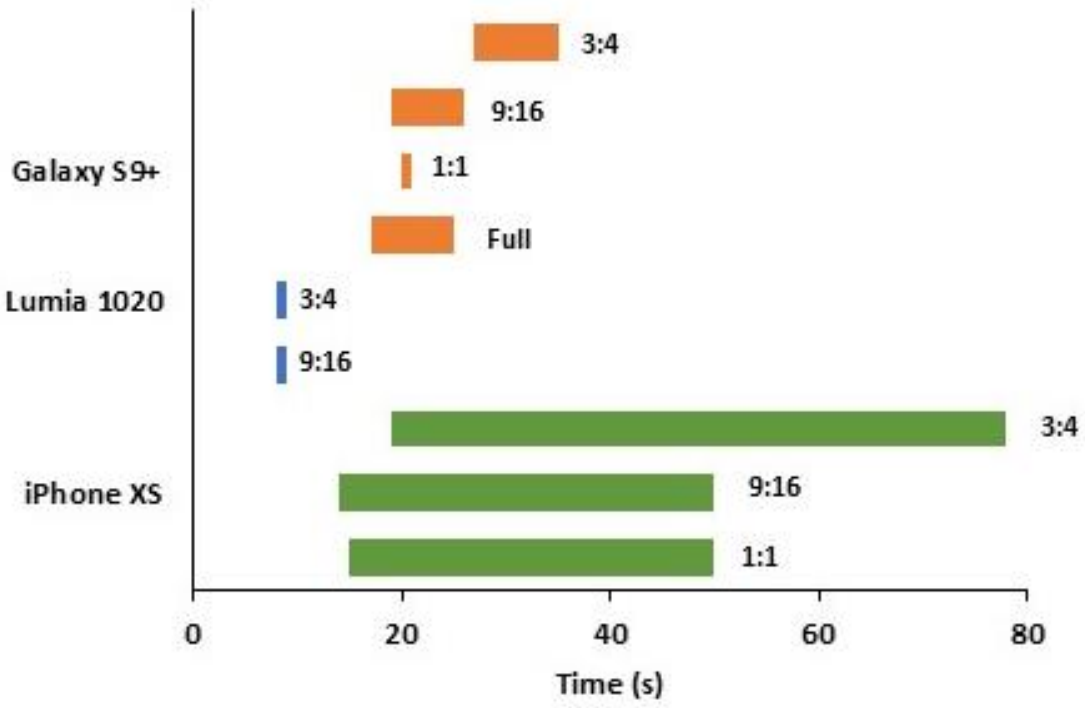

Figure 3-16 Time taken by ANN to quantify images obtained through different smartphones at different digital zooms.

4. PRELIMINARY RESULTS OF LEUKOCYTE QUANTIFICATION

4.1 Microfluidic chip design

A microfluidic chip was designed to process the biological samples and capture the leukocytes present in it. The microfluidic chip contains the capture chamber, which as the name suggests is used to capture the cells of interest i.e. leukocytes, based on antigen antibody interaction. The chamber has a size of 10mm x 4mm and a height of 60 µm. In order to maximize the capture efficiency of the capture chamber, pillars having a diameter of 40 µm and spacing of 17 µm were introduced throughout the chamber design to increase the interaction area between leukocytes and antigens. In total, the capture chamber contains about 13000 pillars which significantly increases the capture efficiency of the chip and minimize the capture of non-specific cells at the same time. The schematic for the microfluidic chip has been shown in Figure 4.1 below.

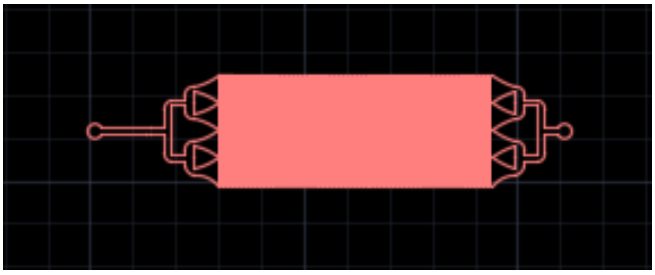

Figure 4-1 Schematic of the microfluidic biochip for capturing leukocytes. Reprinted, with permission, from Ref [23].

4.2 SU-8 master mold

SU-8 2025 from Microchem was used to create a silicon mold for mass production of the microfluidic chip using soft lithography. The thickness of the mold was measured by using a profilometer and it came out to be 60 µm. The

mold was then silanized to make the devices easier to peel off.

4.3 Microfluidic chip fabrication

PDMS devices were then made using this mold by pouring the base and cross linker in a ratio of 10:1. This PDMS mixture was then degassed by placing it in a vacuum desiccator. After removal of the trapped air, the PDMS mixture was baked on a hot plate at 85^{o} C for one hour. Finally, the devices were cut out using a sharp blade and bonded to glass slides using a corona system. The final microfluidic chip is shown in Figure 4.2 and 4.3 below.

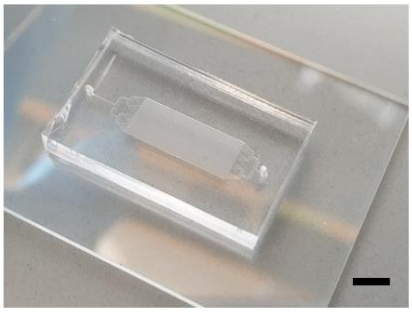

Figure 4-2 Fabricated microfluidic chip made from PDMS bonded to a glass slide. It has holes for fluid inlet and outlet (Scale bar = 5 mm). Reprinted, with permission, from Ref [23].

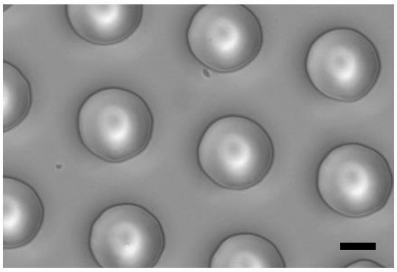

Figure 4-3 The pillars inside the capture chamber of the fabricated PDMS microfluidic chip. The chip is being observed under a brightfield benchtop microscope (Scale bar = 20 μm). Reprinted, with permission, from Ref [23].

4.5 Antibody conjugation in the microfluidic device

To capture leukocytes in the capture chamber, purified anti-human CD45 antibodies were bought from Biolegend (Cat# 368502). These antibodies were then diluted by adding them to PBS in a ratio of 1 to 4 respectively. This diluted antibody solution was then flowed through then biochip and allowed to sit in the capture chamber for one hour to allow for the adsorption of antibodies to capture chamber surface. PBS was then flowed through the chamber again to wash away the free antibodies. This process was then repeated once more to ensure that entire capture chamber surface was covered with antibodies.

4.6 Leukocyte capture in the microfluidic device

Leukocyte solution was flowed through the biochip at a flow rate of 10 µl/min, which resulted in the capture of leukocytes based on antigen antibody interaction. For imaging the captured cells, they were stained with a nuclei acid stain SYTO 16 (Product no. S7578, ThermoFisher). 50 ml of this stain was then injected in the chip at 10 µl/min and incubated in the dark for 15 minutes. Next, to verify the capture of the leukocytes in the microfluidic chip, we imaged the chip under a benchtop fluorescent microscope and observed the captured leukocytes. The brightfield and darkfield images of the captured leukocytes in the microfluidic chip are shown in Figure 4.4.

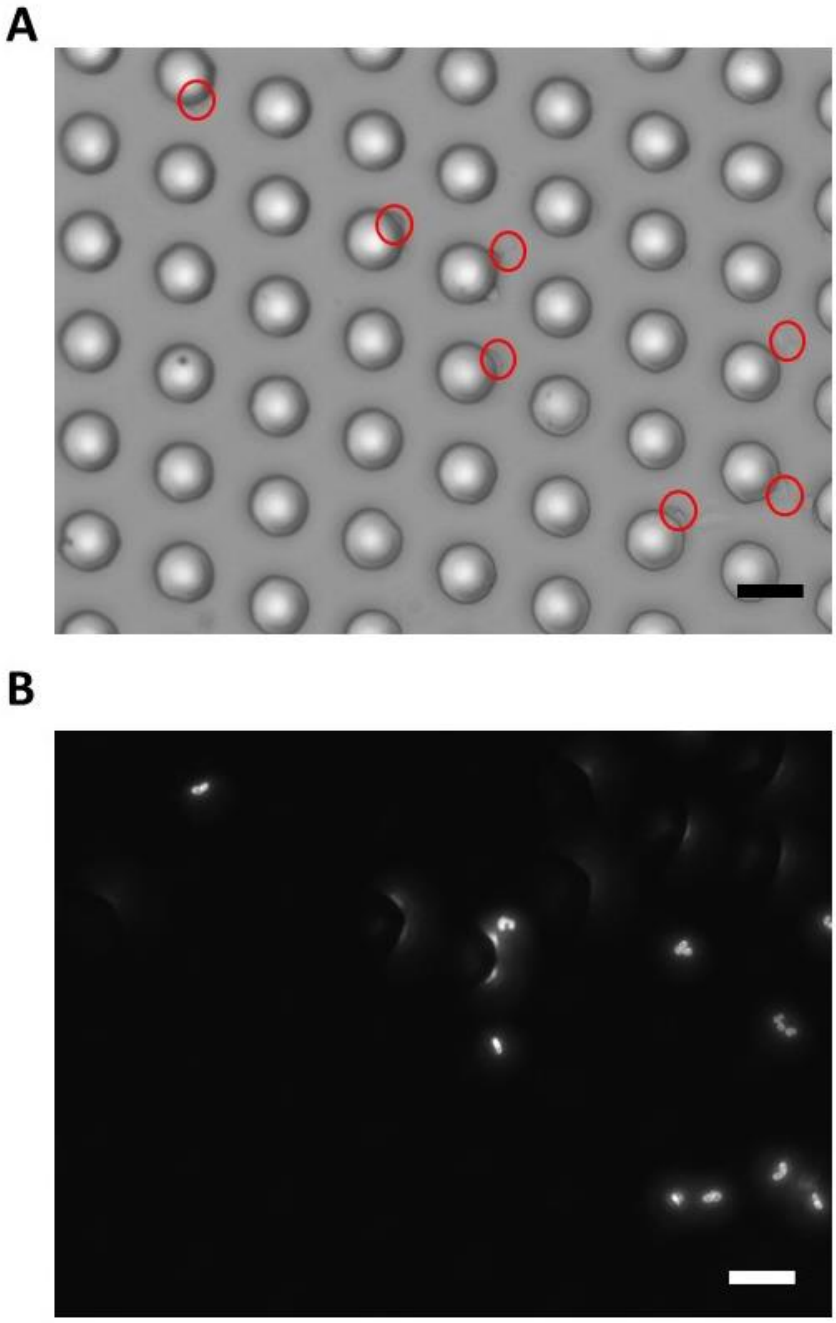

Figure 4-4 a) Microscopic brightfield image of leukocytes captured in biochip. b) Microscopic fluorescent image of captured leukocytes (Scale bar = 50 µm). Reprinted, with permission, from Ref [23].

Next, we put this microfluidic chip inside the SBFM and imaged it using a Samsung Galaxy S9+ along with the 15 mm focal length lens. The resulting image of the captured leukocytes are shown in Figure 4.5 below.

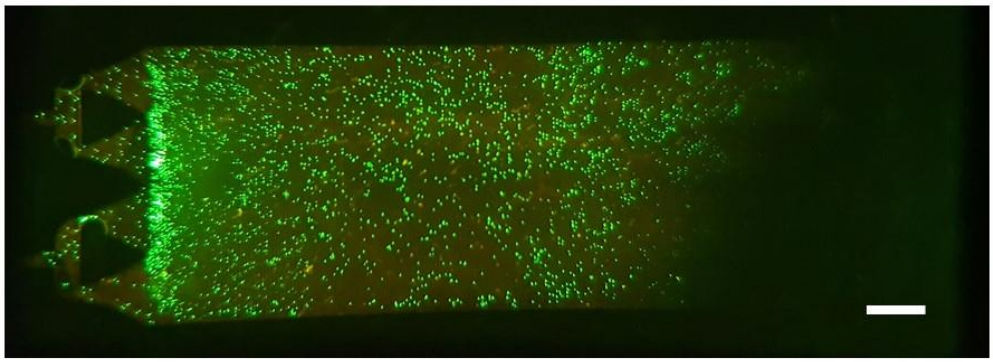

Figure 4-5 Leukocytes captured in the microfluidic chip imaged using the smartphone based fluorescent microscope (Scale bar = 1 mm). Reprinted, with permission, from Ref [23].

5. CONCLUSION AND FUTURE SCOPE

We have presented the design and working of a smartphone based fluorescent microscope. The modular design of the presented SBFM gives the user the capability to easily swap between different sets of lenses and filters and thereby allowing work with different fluorophores at different magnification levels. We then tested the performance of the SBFM against regular benchtop microscope and found it to be satisfactory. To automate the process of fluorescent microparticle quantification, we trained and tested multiple different artificial neural networks and compared their predicted counts against the control method and found their performance to be satisfactory.

We also designed and fabricated a PDMS based microfluidic chip for the quantification of leukocytes in peripheral whole blood and imaged it under the SBFM. By appropriately labelling the capture chamber of the microfluidic chip, we can in future use this device for multiple different applications, such the quantification of CD4/CD8 T-cells or the number of leukocytes in urine samples to assess whether patients have urinary tract infections.

6. APPENDIX

6.1 Resolution measurement protocol

A 1951 USAF resolution test chart from was used to measure the resolution of the designed SBFM. Samsung Galaxy S9+ and Nokia Lumia 1020 were used along with a lens having a focal length of 10 mm and the resolution test chart was imaged by both devices. Pixel intensities of the obtained images were analyzed by using ImageJ to quantify the resolution of the SBFM when used in conjunction with each of these devices.

6.2 Benchtop fluorescent microscope

A benchtop fluorescent microscope was also for imaging the different concentrations of the fluorescent microbeads and leukocytes. For the said purpose, we employed Olympus IX81 fluorescent microscope with a 465-495 nm excitation and 515-555 nm emission filters. Images of the different bead and leukocyte concentrations were obtained from this microscope and were used as a control to quantify the accuracy and precision of the SBFM.

6.3 Polydimethylsiloxane (PDMS)

PDMS is a polymer which is employed widely used in the prototyping and fabrication of microfluidic chips from a master mold. The master mold is generally made using photolithography and uses SU-8. This mater mold is then used for making multiple copies of the device using PDMS. PDMS is nontoxic and bio compatible which is why it finds wide usage in the field of microfluidics. The detailed procedure of making mater molds and PDMS devices is discussed above.

6.4 SU 8 mold fabrication detailed steps

The first step in the process is to clean the silicon wafer. This is done by exposing the silicon wafer to acetone, isopropyl alcohol, and DI water for 10 minutes each. The wafer is then dried using a nitrogen gun and is then hard baked to remove any traces of left-over fluid. Next, we spin coat SU8 photoresist on the silicon wafer and soft bake of the spin coated photoresist at 65 ◦C and 95 ◦C for 2 and 4 minutes, respectively. Further, the wafer is UV Exposed via Chromium mask with exposure dose being 30 mJ/cm2.

After exposure to UV radiation, post exposure baking is done. It is a two-step process and involves heating on a hot plate at 65 ◦C and 95 ◦C for 2 and 6 minutes, respectively.

Next, the silicon wafer is dipped in SU-8 developed for about 7.5 minutes and is stirred constantly to remove the excess traces of SU-8. Finally, the wafer is rinsed and dried using a nitrogen gun. The process flow is shown in Figure 6.1.

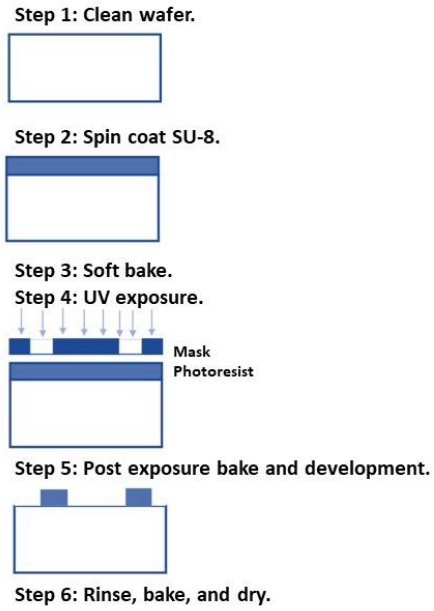

Figure 6-1 SU-8 mold fabrication steps.

7. REFERENCES

[1] Tata, B.; Raj, B., Confocal laser scanning microscopy: Applications in material science and technology. Bulletin of Materials Science 1998, 21 (4), 263-278.

[2] Leung, B. O.; Chou, K. C., Review of super-resolution fluorescence microscopy for biology. Applied spectroscopy 2011, 65 (9), 967-980.

[3] Munné, S.; Grifo, J.; Cohen, J.; Weier, H., Chromosome abnormalities in human arrested preimplantation embryos: a multiple-probe FISH study. American journal of human genetics 1994, 55 (1), 150.

[4] Raj, A.; Van Den Bogaard, P.; Rifkin, S. A.; Van Oudenaarden, A.; Tyagi, S., Imaging individual mRNA molecules using multiple singly labeled probes. Nature methods 2008, 5 (10), 877-879.

[5] Zhu, W.; Gong, C.; Kulkarni, N.; Nguyen, C. D.; Kang, D., Smartphone-based microscopes. In Smartphone Based Medical Diagnostics, Elsevier: 2020; pp 159-175.

[6] Roda, A.; Michelini, E.; Zangheri, M.; Di Fusco, M.; Calabria, D.; Simoni, P., Smartphone-based biosensors: A critical review and perspectives. TrAC Trends in Analytical Chemistry 2016, 79, 317-325.

[7] Ludwig, S. K.; Tokarski, C.; Lang, S. N.; van Ginkel, L. A.; Zhu, H.; Ozcan, A.; Nielen, M. W., Calling biomarkers in milk using a protein microarray on your smartphone. PLoS One 2015, 10 (8), e0134360.

[8] Ludwig, S. K.; Zhu, H.; Phillips, S.; Shiledar, A.; Feng, S.; Tseng, D.; van Ginkel, L. A.; Nielen, M. W.; Ozcan, A., Cellphone-based detection platform for rbST biomarker analysis in milk extracts using a microsphere fluorescence immunoassay. Analytical and bioanalytical chemistry 2014, 406 (27), 6857-6866.

[9] Coskun, A. F.; Nagi, R.; Sadeghi, K.; Phillips, S.; Ozcan, A., Albumin testing in urine using a smart-phone. Lab on a Chip 2013, 13 (21), 4231-4238.

[10] Wei, Q.; Luo, W.; Chiang, S.; Kappel, T.; Mejia, C.; Tseng, D.; Chan, R. Y. L.; Yan, E.; Qi, H.; Shabbir, F., Imaging and sizing of single DNA molecules on a mobile phone. ACS nano 2014, 8 (12), 12725-12733.

[11] Kühnemund, M.; Wei, Q.; Darai, E.; Wang, Y.; Hernández-Neuta, I.; Yang, Z.; Tseng, D.; Ahlford, A.; Mathot, L.; Sjöblom, T., Targeted DNA sequencing and in situ mutation analysis using mobile phone microscopy. Nature communications 2017, 8 (1), 1-8.

[12] Zhu, H.; Sencan, I.; Wong, J.; Dimitrov, S.; Tseng, D.; Nagashima, K.; Ozcan, A., Cost-effective and rapid blood analysis on a cell-phone. Lab on a Chip 2013, 13 (7), 1282-1288.

[13] Koydemir, H. C.; Gorocs, Z.; Tseng, D.; Cortazar, B.; Feng, S.; Chan, R. Y. L.; Burbano, J.; McLeod, E.; Ozcan, A., Rapid imaging, detection and quantification of Giardia lamblia cysts using mobile-phone based fluorescent microscopy and machine learning. Lab on a Chip 2015, 15 (5), 1284-1293.

[14] Wei, Q.; Qi, H.; Luo, W.; Tseng, D.; Ki, S. J.; Wan, Z.; Göröcs, Z. n.; Bentolila, L. A.; Wu, T.-T.; Sun, R., Fluorescent imaging of single nanoparticles and viruses on a smart phone. ACS nano 2013, 7 (10), 9147-9155.

[15] Sung, Y.; Campa, F.; Shih, W.-C., Open-source do-it-yourself multi-color fluorescence smartphone microscopy. Biomedical optics express 2017, 8 (11), 5075-5086.

[16] Dai, B.; Jiao, Z.; Zheng, L.; Bachman, H.; Fu, Y.; Wan, X.; Zhang, Y.; Huang, Y.; Han, X.; Zhao, C., Colour compound lenses for a portable fluorescence microscope.

Light: Science & Applications 2019, 8 (1), 1-13.

[17] Cho, S.; Islas-Robles, A.; Nicolini, A. M.; Monks, T. J.; Yoon, J.-Y., In situ, dual-mode monitoring of organ-on-a-chip with smartphone-based fluorescence microscope. Biosensors and Bioelectronics 2016, 86, 697-705.

[18] Lee, S. A.; Yang, C., A smartphone-based chip-scale microscope using ambient illumination. Lab on a Chip 2014, 14 (16), 3056-3063.

[19] Meng, X.; Huang, H.; Yan, K.; Tian, X.; Yu, W.; Cui, H.; Kong, Y.; Xue, L.; Liu, C.; Wang, S., Smartphone based hand-held quantitative phase microscope using the transport of intensity equation method. Lab on a Chip 2017, 17 (1), 104-109.

[20] Jung, D.; Choi, J.-H.; Kim, S.; Ryu, S.; Lee, W.; Lee, J.-S.; Joo, C., Smartphone-based multi-contrast microscope using color-multiplexed illumination. Scientific reports 2017, 7 (1), 1-10.

[21] Müller, V.; Sousa, J. M.; Koydemir, H. C.; Veli, M.; Tseng, D.; Cerqueira, L.; Ozcan, A.; Azevedo, N. F.; Westerlund, F., Identification of pathogenic bacteria in complex samples using a smartphone based fluorescence microscope. RSC advances 2018, 8 (64), 36493-36502.

[22] Knowlton, S.; Joshi, A.; Syrrist, P.; Coskun, A. F.; Tasoglu, S., 3D-printed smartphone-based point of care tool for fluorescence-and magnetophoresis-based cytometry. Lab on a Chip 2017, 17 (16), 2839-2851.

[23] Sami, M. A.; Wagner, K.; Parikh, P.; Hassan, U. In Smartphone Based Microfluidic Biosensor for Leukocyte Quantification at the Point-of-Care, 2019 IEEE Healthcare Innovations and Point of Care Technologies,(HI-POCT), IEEE: 2019; pp 119-122.

[24] Ghonge, T.; Koydemir, H. C.; Valera, E.; Berger, J.; Garcia, C.; Nawar, N.; Tiao, J.; Damhorst, G. L.; Ganguli, A.; Hassan, U., Smartphone-imaged microfluidic biochip for measuring CD64 expression from whole blood. Analyst 2019, 144 (13), 3925-3935.

[25] Fan, Y.; Yang, C., Competition, Product Proliferation, and Welfare: A Study of the US Smartphone Market. American Economic Journal: Microeconomics 2020, 12 (2), 99-134.

[26]. Sami, M.; Tayyab, M.; Parikh, P.; Govindaraju, H.; Hassan, U. A Modular Microscopic Smartphone Attachment For Imaging And Quantification Of Multiple Fluorescent Probes Using Machine Learning. The Analyst 2021.